



# Assessment of global wave models on regular and unstructured grids using the Unresolved Obstacles Source Term

Lorenzo Mentaschi<sup>1</sup> · Michalis Vousdoukas<sup>1</sup> · Tomas Fernandez Montblanc<sup>2,3</sup> · Georgia Kakoulaki<sup>1</sup> · Evangelos Voukouvalas<sup>4</sup> · Giovanni Besio<sup>5</sup> · Peter Salamon<sup>1</sup>

Received: 1 May 2020 / Accepted: 9 September 2020 / Published online: 24 September 2020  
© The Author(s) 2020

## Abstract

The Unresolved Obstacles Source Term (UOST) is a general methodology for parameterizing the dissipative effects of subscale islands, cliffs, and other unresolved features in ocean wave models. Since it separates the dissipation from the energy advection scheme, it can be applied to any numerical scheme or any type of mesh. UOST is now part of the official release of WAVEWATCH III, and the freely available package *alphaBetaLab* automates the estimation of the parameters needed for the obstructed cells. In this contribution, an assessment of global regular and unstructured (triangular) wave models employing UOST is presented. The results in regular meshes show an improvement in model skill, both in terms of spectrum and of integrated parameters, thanks to the UOST modulation of the dissipation with wave direction, and to considering the cell geometry. The improvement is clear in wide areas characterized by the presence of islands, like the whole central-western Pacific Basin. In unstructured meshes, the use of UOST removes the need of high resolution in proximity of all small features, leading to (a) a simplification in the development process of large scale and global meshes, and (b) a significant decrease of the computational demand of accurate large-scale models.

**Keywords** Wave modeling · Global wave modeling · Subscale modeling · Unresolved obstacles · Unresolved Obstacles Source Term · UOST · WAVEWATCH III · WW3 · Global unstructured mesh · Global triangular mesh

---

This article is part of the Topical Collection on the *16th International Workshop on Wave Hindcasting and Forecasting in Melbourne, AU, November 10–15, 2019*

---

Responsible Editor: Jenny M Brown

---

**Electronic supplementary material** The online version of this article (<https://doi.org/10.1007/s10236-020-01410-3>) contains supplementary material, which is available to authorized users.

---

✉ Lorenzo Mentaschi  
Lorenzo.MENTASCHI@ec.europa.eu

- <sup>1</sup> Joint Research Centre (JRC), European Commission, Ispra, Italy
- <sup>2</sup> Department of Physics and Earth Sciences, Università degli Studi di Ferrara, Via Saragat, 1, 44122 Ferrara, Italy
- <sup>3</sup> Department of Earth Sciences, University of Cádiz, Avda. República Saharaui s/n, Puerto Real 11510 Cádiz, Spain
- <sup>4</sup> Unisystems Luxembourg Sàrl, Luxembourg, Luxembourg
- <sup>5</sup> Dipartimento di Ingegneria Chimica, Civile ed Ambientale (DICCA), Università di Genova, Genova, Italy

## 1 Introduction

The dissipative effect of unresolved islands and small obstacles is a major source of error in wave models if neglected, both locally and on large scale. This is more evident in basins characterized by the presence of large number of islands, such as the Pacific Ocean or the Baltic Sea (Tolman 2003; Tuomi et al. 2014). The most established approach to tackle this problem is the attenuation of the wave energy traveling through the obstructed cells, as a function of transparency coefficients. Such approach is traditionally implemented in the numerical scheme modeling the spatial propagation of the waves (Booij et al. 1999; Tolman 2003; Chawla and Tolman 2008). The above studies typically consider 2 transparency coefficients, one for energy traveling along each Cartesian direction ( $x$  and  $y$ ) of regular meshes. However, Hardy and Young (1996) and Hardy et al. (2000) showed the advantages of modulating the attenuation with wave direction, as small islands with irregular and elongated shape can lead to a non-isotropic dissipation of energy. The approach they proposed, which is based on the advection scheme and

considers the wave direction, is currently implemented in the model ECWAM (ECMWF 2019).

More recently, Mentaschi et al. (2015) theorized a methodology for subscale modeling the dissipation due to unresolved obstacles based on source terms (the Unresolved Obstacles Source Term, hereinafter referred to as UOST). Given each cell of a mesh, UOST estimates, for each spectral component, the dissipative effect of the unresolved features located in the cell (local dissipation), and the shadow projected to the downstream cells (shadow effect, SE). The source term can be expressed as:

$$S_{uo} = S_{ld} + S_{se}, \quad (1)$$

$$S_{ld} = -\psi_{ld} \frac{1-\beta_l}{\beta_l} \frac{c_g}{\Delta L} N, \quad (2)$$

$$S_{se} = -\psi_{se} \left( \frac{\beta_u}{\alpha_u} - 1 \right) \frac{c_g}{\Delta L} N, \quad (3)$$

where  $S_{ld}$  and  $S_{se}$  are the local dissipation and the shadow effect,  $N$  is the spectral density,  $c_g$  is the group velocity,  $\Delta L$  is the path length of the spectral component in the cell, and the  $\psi$  factors model the reduction of the dissipation in presence of local wave growth. The subscripts  $l$  and  $u$  of  $\alpha$  and  $\beta$  indicate that these transparency coefficients can be referred, respectively, to the cell and to the upstream polygon. For a more detailed explanation on the theoretical framework of UOST, the reader is referred to Mentaschi et al. (2015, 2018). Appendix provides a discussion on the geometrical meaning of the coefficients  $\alpha$  and  $\beta$ .

The viability of UOST in real-world applications on regular meshes was shown by Mentaschi et al. (2018), and an open-source software package for the automatic computation of the transparency coefficients needed by UOST was developed (*alphaBetaLab*, now supporting regular and triangular meshes, Mentaschi et al. 2019). Furthermore, UOST is now part of release 6.07 of the wave model WAVEWATCH III (hereinafter referred to as WW3, WW3DG 2019).

A significant benefit of using UOST with respect to other implementations is that it considers the swell direction and the layout of the obstacles in the obstructed cells. Furthermore, it can be applied with any type of mesh and numerical scheme, and this is useful as the number of solvers of the wave action equation is constantly increasing, the numerical schemes are becoming more and more sophisticated (e.g., Roland 2008; Zijlema 2010; Li 2011), and in some cases, parameterizing the effect of the unresolved obstacles within the scheme would not be straightforward.

In this contribution, we illustrated the abovementioned advantages by running and validating global models on both unstructured and regular meshes with UOST, and comparing against simulation results using the numerical scheme-based approach implemented in WW3 for regular

grids (hereinafter referred to as GRIDGEN, Chawla and Tolman 2008), as well as without any parameterization of the unresolved obstacles.

Section 2 of the manuscript describes the model setup and the validation methodology employed in this study. Section 3 summarizes the results, which are discussed in more detail in Section 4. Final remarks are drawn in Section 5.

## 2 Model setup and validation

In this study, the wave model WW3 version 6.07 was implemented over regular and unstructured (triangular) global domains, forced by 6-h 10 m winds from the Climate Forecast System Reanalysis (CFSR Saha et al. 2010). The spectral grid is constant for all the simulations, with a directional resolution of  $15^\circ$  and 25 frequency bands ranging exponentially from 0.04 to 0.5 Hz, separated by a factor of 1.1. The parameterization of the physics of wave growth/dissipation as proposed by Ardhuin et al. (2010), hereinafter referred to as ST4, was employed. The wave growth tuning parameter BETAMAX was set to 1.33, a value suggested by WW3DG (2019) for CFSR wind data. The Discrete Interaction Approximation (DIA) was used to represent the non-linear interactions (Hasselmann and Hasselmann 1985). Although shallow water dynamics are not expected to play a significant role at the spatial scales examined in this manuscript, the model setup includes the JONSWAP parameterization for bottom friction (Hasselmann et al. 1973), and the approach of Battjes and Janssen (1979) for surf breaking. UOST was set up by compiling the executables with the corresponding WW3 switch, and post-processing the meshes with the *alphaBetaLab* utility (Mentaschi et al. 2019, see Appendix for details).

The two regular meshes employed in this study cover the globe (latitude  $80^\circ$  S– $80^\circ$  N) with resolutions of  $1.5^\circ$  and  $0.4^\circ$  respectively, and the ULTIMATE QUICKEST numerical scheme (Leonard 1991) was used for energy propagation. The global unstructured mesh has a resolution of about 150 km ( $\sim 1.5^\circ$ ) offshore and 10 km ( $\sim 0.1^\circ$ ) nearshore, and the implicit N-scheme was employed (Zijlema 2010; Roland 2012). The values of the global time step, and of the time steps of spatial and spectral propagation, were set to 900 s, 300 s and 300 s respectively for all the models. Such value of the global time step guarantees an accurate application of UOST in cells with a length  $> \sim 15$  km in the direction of the wave propagation (Mentaschi et al. 2018). The simulations were carried out on a 10-year time frame (2000–2009) using different approaches for the parameterization of the unresolved obstacles: no parameterization (hereinafter no subscale modeling, NOSM), UOST, and, for regular domains, GRIDGEN (Table 1). Maps of bulk wave parameters (significant wave height  $H_s$ , mean period  $T_{0.1}$ ) were saved hourly for all the

**Table 1** Simulations carried out, mesh type employed parameterization of the unresolved obstacles

Simulation ID	Mesh type	Unresolved obstacles parameterization
NOSM-UNST	Unstructured	None
UOST-UNST	Unstructured	UOST
NOSM-150	Regular 1.5°-res.	None
GRIDGEN-150	Regular 1.5°-res.	GRIDGEN
UOST-150	Regular 1.5°-res.	UOST
NOSM-040	Regular 0.4°-res.	None
GRIDGEN-040	Regular 0.4°-res.	GRIDGEN
UOST-040	Regular 0.4°-res.	UOST

simulations, while the spectra were stored at selected locations.

The accuracy of the runs was evaluated versus satellite altimeter data of  $H_s$  provided by the Globwave database (Queffeuou and Croizé-Fillon 2014). The dataset includes altimeter data from various satellites: ERS 1 and 2, ENVISAT, GEOSAT, Jason 1 and 2, Poseidon, TOPEX, and Cryosat 2. Since the resolution of the satellite data along the satellite tracks is much higher than that of the model runs, satellite data have been aggregated on 0.5°-long segments along the tracks and averaged. The model output was space-time interpolated to the corresponding points along the tracks and compared with the satellite observation. Wave heights lower than 0.5 m in either model or observations were excluded from the validation, due to the unreliability of the measurements for low values of  $H_s$ . The pairs simulation-observation were grouped in 1°-sided tiles, and these statistical indicators were used as proxies of performance:

$$NBI = \frac{\sum(S_i - O_i)}{\sum O_i}, \tag{4}$$

$$NRMSE = \sqrt{\frac{\sum(S_i - O_i)^2}{\sum O_i^2}}, \tag{5}$$

where  $S$  represents the simulated value of  $H_s$ ;  $O$  represents the observation.

### 3 Results

On a regular mesh with a resolution of 1.5°, a model without subscale modeling has a mean positive bias of little less than 10% of  $H_s$ , exceeding 30% in vast areas characterized by the presence of many islands, like the tropical western part of the Pacific basin (Fig. 1a). Employing GRIDGEN considerably improves the bias, lowering it to 1.5%, while the NRMSE decreases from 17.5 to 14.2%. However, we notice that GRIDGEN-150 underestimates  $H_s$  in many areas, with a negative bias below - 10% in vast portions of the Pacific Ocean,

and other areas filled with islands (Fig. 1b). The model employing UOST results in an overall bias similar to GRIDGEN, but with a narrower spatial distribution and fewer areas affected by relevant underestimation of  $H_s$ . The overall value of NRMSE is consequently reduced further to 13.7% (Fig. 1c).

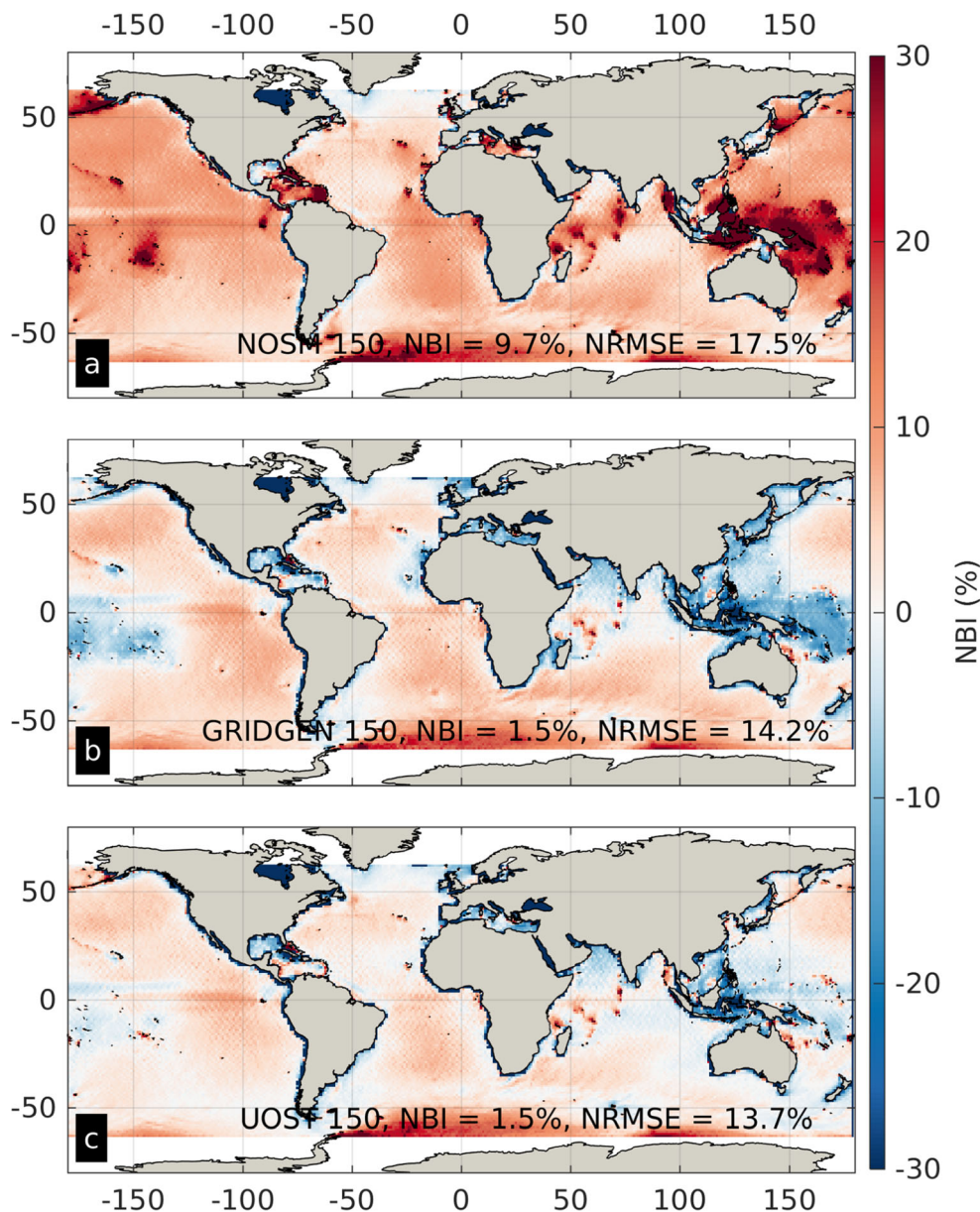
The results are similar for the simulations with the 0.4° regular mesh and on the unstructured mesh, though with biases of  $H_s$  reduced with respect to NOSM-150. For NOSM-040 (NOSM-UNST), the overall overestimation of  $H_s$  is 5.3% (2.6%), with local exceedance beyond 20% in many areas (Figs. 2a and 3a). Both GRIDGEN and UOST reduce such kind of overestimation, but at 0.4° as at 1.5° GRIDGEN comes with an underestimation of  $H_s$  in the western Pacific Basin and in other areas filled with islands (Fig. 2b). While in UOST-040 such negative bias is smaller, and in UOST-UNST is absent (Figs. 2c and 3b).

### 4 Discussion

The importance of taking into consideration the unresolved obstacles is shown by the better skill of models adopting any approach for subscale modeling, with respect to models neglecting them, for all the considered meshes. In particular, the skill of a 1.5° model on a regular mesh with GRIDGEN or UOST is better than that of a 0.4° model without. This fact is remarkable if one considers that a 0.4° simulation is about 14 times more expensive than a 1.5° one, from a computational point of view. Similar considerations hold comparing the 1.5° simulations with the ones of the unstructured mesh. Moreover, coarse resolutions as for example 1.5° are viable to provide boundary conditions to higher resolution local models, to perform climate projections, and in general in applications where the exact knowledge of the wave climate in specific locations and at specific times is not required.

The skill improvement in models adopting any approach for subscale modeling is also noticeable for the higher

**Fig. 1** Normalized bias (NBI) of  $H_s$  for simulations on the  $1.5^\circ$ -resolution domain. No subscale modeling (a), GRIDGEN (b), UOST (c). The red (blue) color indicates overestimation (underestimation) of  $H_s$



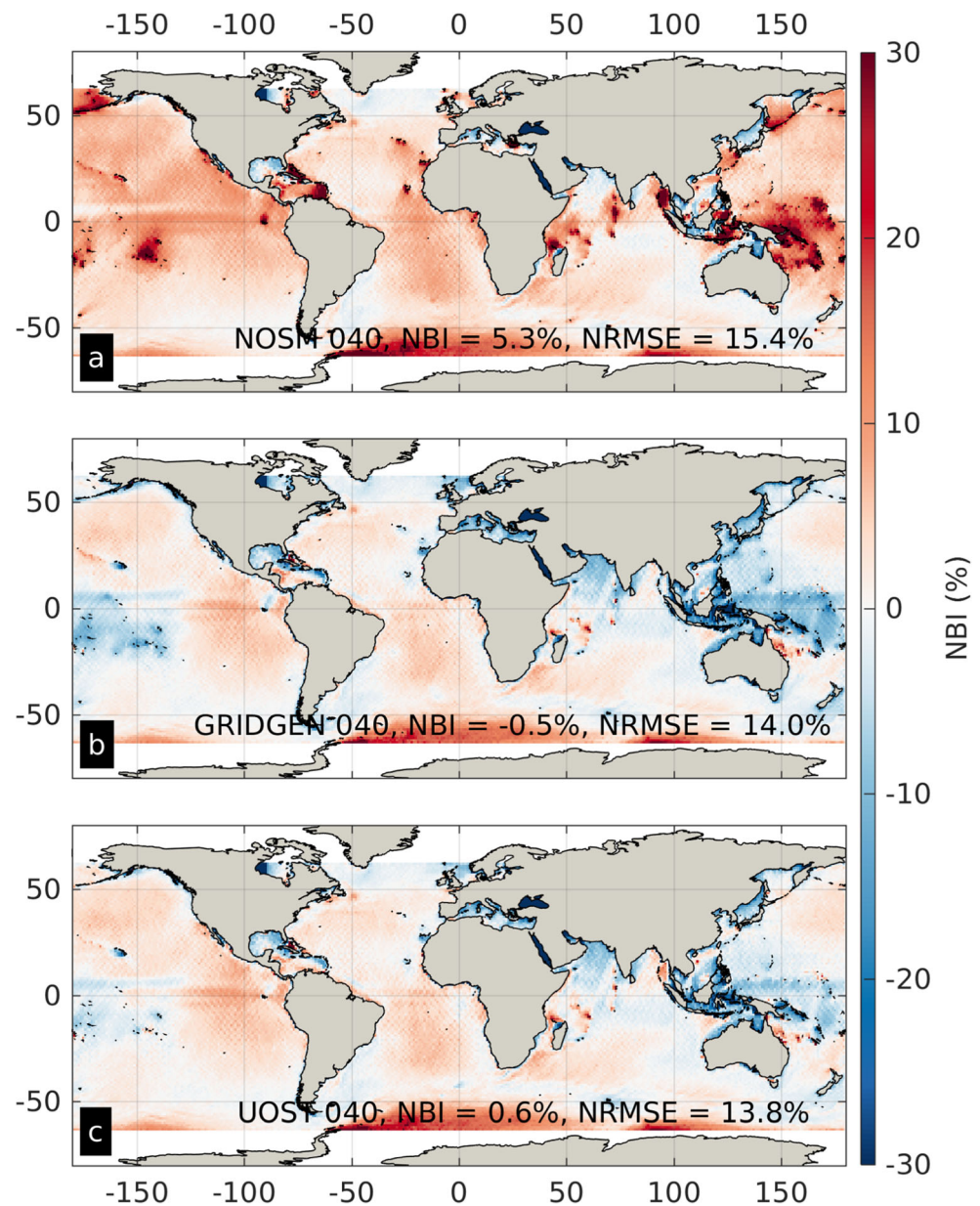
resolution domains (040 and UNST) and can be dominant in many locations, especially in the presence of intense swell events. For example, during a swell event in the shadow area of the Palliser Islands on 23/02/2008, NOSM-040 modeled values of  $H_s$  ( $T_{0-1}$ ) about 75% (35%) larger than UOST-040 and about twice larger than GRIDGEN-040. Accordingly, the peak of frequency spectrum modeled by NOSM-040 is 4.8 times larger than that of UOST-040, and  $\sim 10$  times larger than that of GRIDGEN-040 (Fig. 4).

The unstructured meshes allow the increase of the resolution in areas of interest for specific applications, potentially ensuring accurate results with respect to regular domains, for the same computational costs. In the unstructured mesh

considered in this study, we reached higher resolutions along the coast than in our regular domains (about 10 km, or  $0.1^\circ$ , versus  $0.4^\circ$  and  $1.5^\circ$ ). A lower (but still noticeable) global impact of the unresolved obstacles than in the regular domains is therefore expected (the global mean NBI of  $H_s$  is 2.6% for NOSM-UNST, versus 0.5% for UOST-UNST). Yet, employing UOST leads to major improvements in large basins characterized by the presence of many small islands, such as the whole Pacific Ocean, where the overestimation of  $H_s$  is reduced from approximately 4% to about 0% (Fig. 3). We remark that UOST is the only workable methodology for subscale modeling the unresolved obstacles on unstructured meshes. It comes with advantages with respect to the usual



**Fig. 2** Same as in Fig. 1, for the 0.4°-resolution simulations

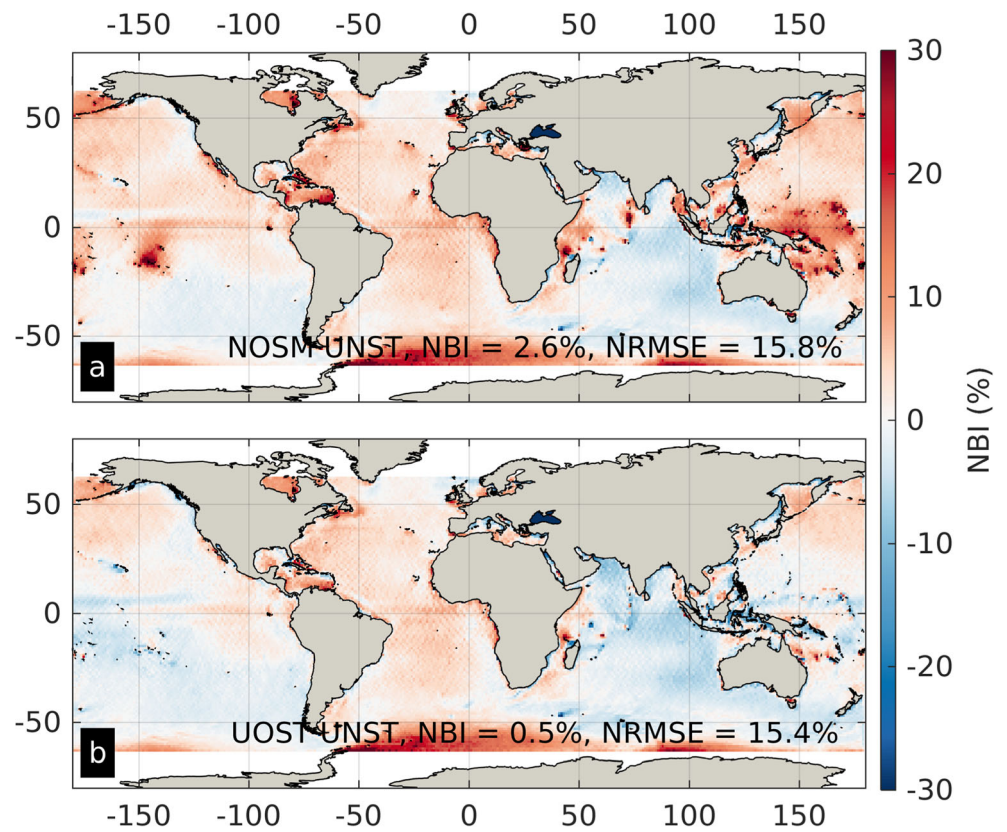


approach of increasing the resolution in proximity of (the majority of) the small islands, which would result in large meshes, expensive from the point of view of development, computation, and storage requirement for the output. The unstructured mesh employed in this study has computational costs and model skills comparable to the ones of the 0.4°-resolution regular mesh, but with higher resolution near the coast representing the nearshore dynamics in higher detail. In that respect, UOST can simplify the process of setting up and running large-scale unstructured meshes: a modeler can increase the resolution in the areas of interest for a specific

application, letting UOST doing its job in areas where only an adjustment of the energy fluxes is needed.

Our results show that UOST can improve the model skill also on regular meshes: GRIDGEN comes with a significant underestimation of Hs at the obstructed cells, which is reduced in UOST (Figs. 1b, c and 2b, c). Such negative bias is most likely due to an overestimation of the dissipation in presence of “diagonal” swell, i.e., with direction angled with respect to the two main axes of the mesh (longitude and latitude). The difference in behavior between UOST and GRIDGEN is exemplified by the two swell events discussed above, the first

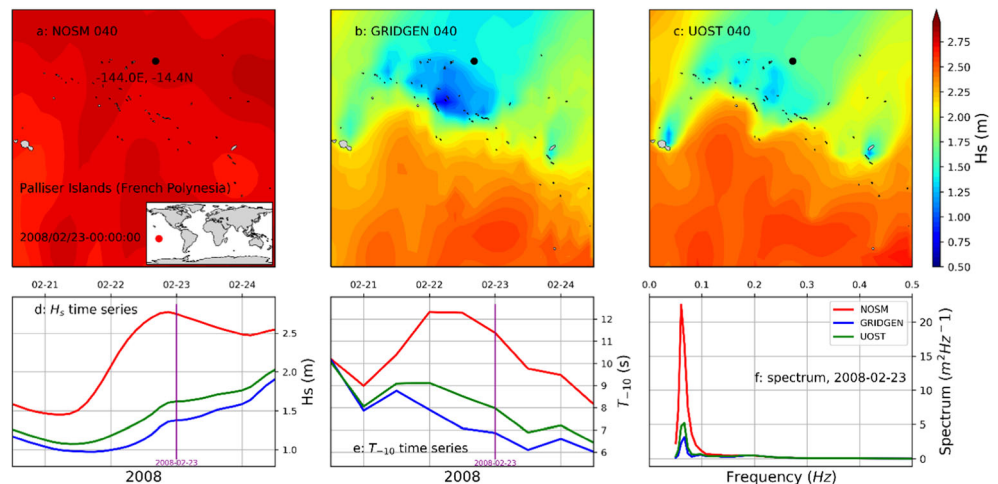
**Fig. 3** Unstructured model bias, without subscale modeling (a) and with UOST (b). The red (blue) color indicates overestimation (underestimation) of  $H_s$



with waves directed diagonally towards NE, at the Palliser Islands (French Polynesia, Fig. 4), the second with westward waves at the Hawaii islands (“straight” swell, Fig. 5). For the event at Hawaii, we notice that GRIDGEN and UOST behave closely, reproducing similar patterns and alike values of  $H_s$ ,  $T_{10}$ , and frequency spectra. On the other hand, for the diagonal event at the Palliser Islands, the dissipation modeled by GRIDGEN is consistently stronger than that of UOST.

The over-dissipation of GRIDGEN with diagonal swells could be related to the fact that it modulates the attenuation only along the 2 main axes of the grid. To reproduce the propagation of diagonal swell, the numerical scheme ULTIMATE QUICKEST decomposes the advection of the wave action into its two components along the zonal and meridional axes, then applies the transparency coefficients estimated for these directions. Even in the case of isotropic cir-

**Fig. 4** Swell event at the Palliser Islands (French Polynesia). Maps of  $H_s$  on 23/02/2008, for NOSM-040 (a), GRIDGEN-040 (b), and UOST-040 (c). Time series of  $H_s$  (d)  $T_{10}$  (e), and frequency spectra at 23/02/2008 (f). The red dot in the planisphere inset in (a) corresponds to the location of the Palliser Islands





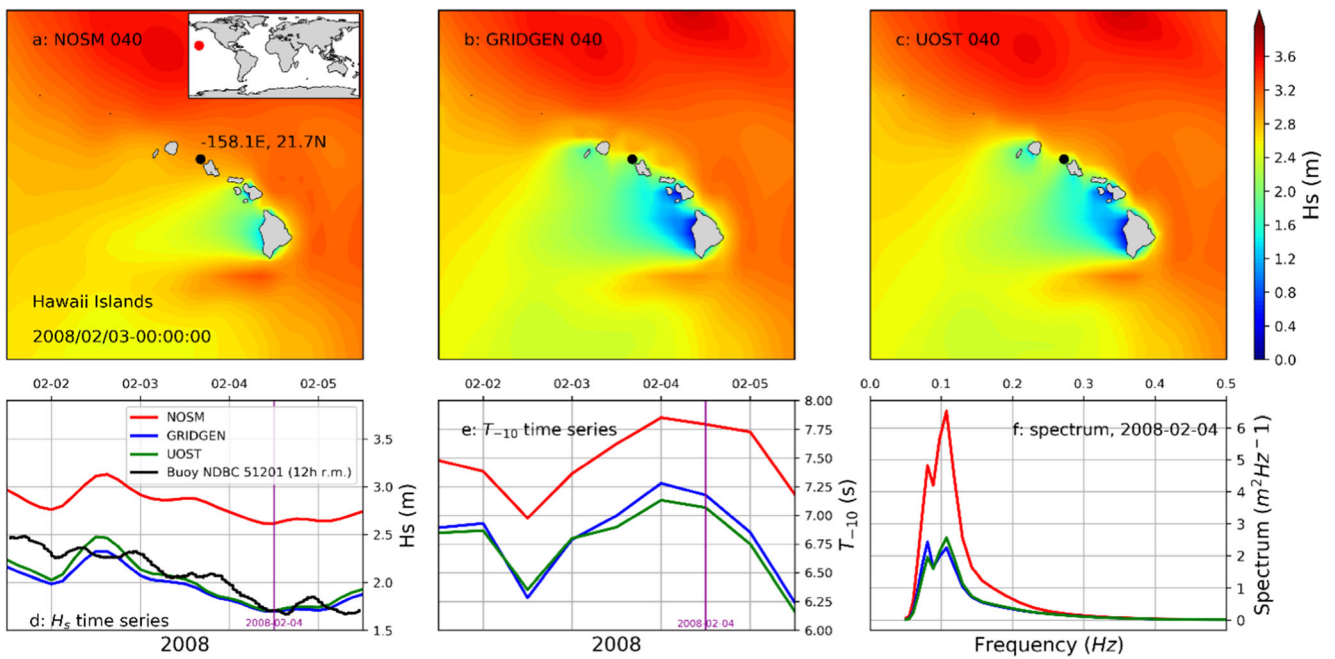
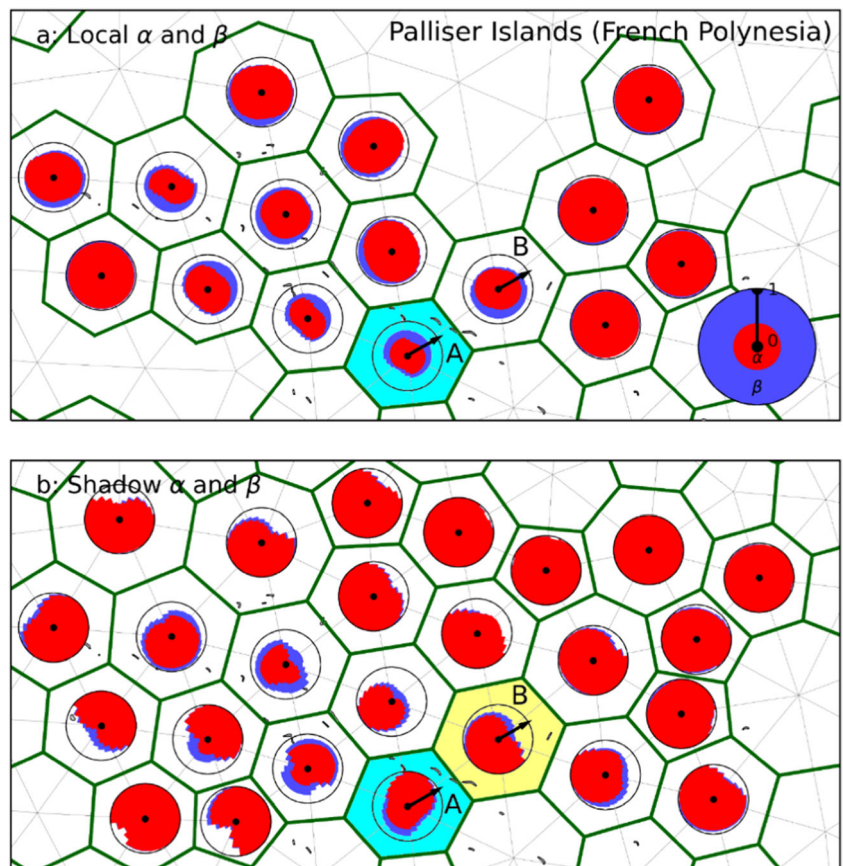


**Fig. 5** Same as in Fig. 4, for a swell event in Hawaii on 03/02/2008. A comparison with the measurements of  $H_s$  of the NDBC buoy 51201 is shown in panel d

**Fig. 6** Excerpt on the Palliser Islands (French Polynesia) of the  $\alpha$  and  $\beta$  coefficients estimated by alphaBetaLab for the unstructured mesh, (a) for local dissipation, (b) for the shadow. The green lines represent the mesh polygons corresponding with the median dual cells. The black dots inside each cell are the mesh nodes. The thin gray lines represent the triangles. In the pies, the red and blue values are respectively the directional  $\alpha$  and  $\beta$  coefficients (notice that  $\beta \geq \alpha$  always). The blue-red circle in the low-right part of panel a is the legend. The physical meaning of  $\alpha$  and  $\beta$  in the cells A and B, for a swell directed like the arrows, is explained in the text



lar unresolved islands, with a dissipative effect independent on the direction, this approach can lead to over-dissipation in regular grids, as the cross section of a circular island computed with respect to the cell side (i.e., for straight swell) is larger than that computed with respect to the cell diagonal, (i.e., for diagonal swell). In other words, UOST allows to better consider not only the geometry of the obstacles, but also the geometry of the cells, which can have different crosswise sizes for swells coming from different directions.

## 5 Final remarks

In this study, we investigate applications of UOST on global domains, showing how it can benefit the model skill on both structured and unstructured meshes. On regular grids, UOST provides a better parameterization of the unresolved obstacles with respect to approaches which only consider the 2 main axes of propagation, as it better modulates the energy dissipation with the swell direction. This is important not only to take into account the geometry of the small islands, which can dissipate different amounts of energy from different directions. It also allows to better consider the geometry of the cell, which can have different crosswise sizes for swells coming from different directions. Neglecting the geometry of the cells is believed to be the cause of the over-dissipation of GRIDGEN in many areas, which is consistently reduced in UOST.

For unstructured (triangular) meshes, UOST comes as the only possible way to subscale model the unresolved obstacles. To show its capability in this context, we employed a mesh with a relatively high resolution along the coasts (about 10 km) but neglecting the plethora of small islands present in the Pacific Ocean and in other basins. UOST consistently improved the model skill with respect to simulations not considering the effects of the unresolved obstacles, by eliminating the overestimation of  $H_s$  in wide portions of the domain. Therefore, UOST opens a new way of wave modeling on unstructured meshes, whereby the mesh resolution is not anymore required to fit the size of small features that might disrupt the flux of wave action: a modeler can refine the mesh where and up to the resolution required by the specific application, leaving to UOST the job on the coarser cells.

## Appendix. *alphaBetaLab* and UOST setup

Two transparency coefficients are required by UOST for each obstructed cell: the total transparency  $\alpha$  to a given spectral component ( $\alpha = 1$  if no obstruction exists,  $\alpha = 0$  if the cell is totally obstructed), and a transparency  $\beta$  that takes into account the distribution of the obstacles inside the cell:  $\beta \sim \alpha$

if the obstacles are close to the upstream side of the cell,  $\beta \sim 1$  if they are close to the downstream side. Furthermore, two sets of  $\alpha$  and  $\beta$  are needed: one for the obstructed cell itself, for the estimation of the local dissipation (LD); the second for the polygon casting a shadow on a cell, for the estimation of the shadow effect (SE).

The software package *alphaBetaLab* was developed to automatize the estimation of  $\alpha$  and  $\beta$  for the obstructed cells (Mentaschi et al. 2019), and was employed in this study to post-process the meshes. The library includes a utility (*alphaBetaLab.plot.alphaBetaPlotter*) which allows visualizing and diagnosing the output of *alphaBetaLab*. Using this module, we could plot the mesh polygons representing the cells in the algorithm, and the values of  $\alpha$  and  $\beta$  estimated for each direction, for both local dissipation and shadow. As an example, an excerpt of the unstructured mesh on the Palliser Islands (French Polynesia) is shown in Fig. 6. In *alphaBetaLab*, the median dual cells of the unstructured mesh are approximated as the polygons connecting the centroids of the triangles (thick green polygons in Fig. 6). Values of  $\alpha$  and  $\beta$  close to 1 indicate that the unresolved obstacles have no effect on the energy flux in a certain direction, while values close to 0 indicate almost total dissipation (red and blue pies in Fig. 6).

We can better understand the geometrical meaning of  $\alpha$  and  $\beta$  by examining their values in cells A and B for swell propagating in direction NE (Fig. 6). Cell A is characterized by the presence of islands aligned in direction NW-SE, and this comes with a stronger dissipation for swell propagating in direction SW-NE (see the orientation of the red pie in cell A, Fig. 6a). The islands are close to the NE side of A, meaning that they have limited effect on the energy coming into A from SW, but affect the energy exiting A towards NE. That's why the value of the LD  $\beta$  of A, for swell propagating towards NE, is significantly larger than the LD  $\alpha$ , while for swell propagating towards SW, it is approximately equal to  $\alpha$  (blue pie in cell A, Fig. 6a). The fact that the islands are located close to the NE side of A means that they project a shadow to cell B, for swell propagating towards NE. That's why the shadow  $\alpha$  and  $\beta$  of B, for swell coming from A, are significantly smaller than 1 (red and blue pies in cell B, Fig. 6b).

**Open Access** This article is licensed under a Creative Commons Attribution 4.0 International License, which permits use, sharing, adaptation, distribution and reproduction in any medium or format, as long as you give appropriate credit to the original author(s) and the source, provide a link to the Creative Commons licence, and indicate if changes were made. The images or other third party material in this article are included in the article's Creative Commons licence, unless indicated otherwise in a credit line to the material. If material is not included in the article's Creative Commons licence and your intended use is not permitted by statutory regulation or exceeds the permitted use, you will need to obtain permission directly from the copyright holder. To view a copy of this licence, visit <http://creativecommons.org/licenses/by/4.0/>.



## References

- Ardhuin F, Rogers E, Babanin AV et al (2010) Semiempirical Dissipation source functions for ocean waves. Part I: definition, calibration, and validation. *J Phys Oceanogr* 40:1917–1941
- Battjes JA, Janssen JPFM (1979) Energy Loss and set-up due to breaking of random waves. In: *Proceedings of the Coastal Engineering Conference*. American Society of Civil Engineers, New York, pp 569–587
- Booij N, Ris RC, HL H (1999) A third generation wave model for coastal regions, part I, model description and validation. *J Geophys Res* 7: 649–666
- Chawla A, Tolman HL (2008) Obstruction grids for spectral wave models. *Ocean Model* 22:12–25. <https://doi.org/10.1016/j.ocemod.2008.01.003>
- ECMWF (2019) Part VII: ECMWF wave model. In: *IFS Documentation CY46R1*
- Hardy TA, Young IR (1996) Field study of wave attenuation on an offshore coral reef. *J Geophys Res* 14:311–326
- Hardy TA, Mason BL, McConochie JD (2000) A wave model for the great barrier reef. *Ocean Eng* 28:45–70
- Hasselmann S, Hasselmann K (1985) Computations and parametrizations of the nonlinear energy transfer in a gravity-wave spectrum. I: a new method for efficient computations of the exact nonlinear transfer integral. *J Phys Oceanogr* 15:1369–1377
- Hasselmann K, Barnett TP, Bouws E et al (1973) Measurements of wind-wave growth and swell decay during the Joint North Sea Wave Project (JONSWAP). *Ergnzungsh zur Dtsch Hydrogr Zeitschrift R* 8:95
- Leonard BP (1991) The ULTIMATE conservative difference scheme applied to unsteady one-dimensional advection. *Comput Methods Appl Mech Eng* 88:17–74
- Li J-G (2011) Global transport on a spherical multiple-cell grid. *Mon Weather Rev* 139:1536–1555. <https://doi.org/10.1175/2010MWR3196.1>
- Mentaschi L, Pérez J, Besio G et al (2015) Parameterization of unresolved obstacles in wave modelling: a source term approach. *Ocean Model* 96:93–102. <https://doi.org/10.1016/j.ocemod.2015.05.004>
- Mentaschi L, Kakoulaki G, Vousedoukas MI et al (2018) Parameterizing unresolved obstacles with source terms in wave modeling: a real-world application. *Ocean Model* 126:77–84. <https://doi.org/10.1016/j.ocemod.2018.04.003>
- Mentaschi L, Vousedoukas M, Besio G, Feyen L (2019) alphaBetaLab: automatic estimation of subscale transparencies for the Unresolved Obstacles Source Term in ocean wave modelling. *SoftwareX* 9:1–6. <https://doi.org/10.1016/j.softx.2018.11.006>
- Queffelec P, Croizé-Fillon D (2014) Global altimeter SWH data set. Laboratoire d’Océanographie Spatiale, IFREMER
- Roland A (2008) Development of WWM II: Spectral wave modelling on unstructured meshes. Technische Universität Darmstadt, Institute of Hydraulic and Water Resources Engineering
- Roland A (2012) Application of residual distribution (RD) schemes to the geographical part of the wave action equation. In: *Proceedings of ECMWF workshop on ocean wave forecasting*
- Saha S, Moorthi S, Pan H-L et al (2010) The {NCEP} Climate Forecast System Reanalysis. *Bull Am Meteorol Soc* 91:1015–1057
- The WAVEWATCH III Development Group (WW3DG) (2019) User manual and system documentation of WAVEWATCH III version 6.07
- Tolman HL (2003) Treatment of unresolved islands and ice in wind wave models. *Ocean Model* 5:219–231
- Tuomi L, Pettersson H, Fortelius C et al (2014) Wave modelling in archipelagos. *Coast Eng* 83:205–220
- Zijlema M (2010) Computation of wind-wave spectra in coastal waters with SWAN on unstructured grids. *Coast Eng* 57:267–277. <https://doi.org/10.1016/j.coastaleng.2009.10.011>